18th Australasian Fluid Mechanics Conference
Launceston, Australia
3-7 December 2012

Drop Interactions in Transient Flows with Applications to Liquid Sprays

V. Magi[1,2] and J. Abraham[1, 3]

[1]School of Mechanical Engineering
Purdue University, West Lafayette, Indiana 47907-2088, USA

[2]Department of Environmental Engineering and Physics
University of Basilicata, 85100 Potenza, Italy

[3]School of Mechanical Engineering
University of Adelaide, Adelaide, South Australia 5005, Australia

Abstract

The behavior of isolated drops, and binary and ternary systems of drops moving in tandem, in decelerating flows are numerically studied employing a finite-volume interface-tracking numerical scheme and a lattice-Boltzmann method for two-phase flows. The influence of Weber and Ohnesorge numbers, separation distance between drops, and drop size-ratio on the transient deformation and breakup of the drops are discussed. Drag coefficients for the drops are also reported. It is shown that in binary drops, the trailing drop decelerates slower than the leading one and breaks up slower. Both drops decelerate slower than the isolated drop. In the case of ternary drops, the three drops decelerate slower than the isolated one. The leading drop breaks up fastest followed by the middle one. The drag coefficients are transient and vary significantly from those of spheres in transient flows as a result of drop deformation.

Introduction

Drops and systems of drops are encountered in many applications. The focus in this manuscript is on liquid fuel sprays where the injection of the liquid leads to atomization which generates drops [7,11]. The injected liquid normally exits the injector orifice at high velocity and subsequently the jet velocity decreases as the liquid shares its momentum with the ambient gas. In this sense, the drops are in a decelerating flow. Flow deceleration leads to significant forces that influence the drop and this can lead to drop deformation and possibly drop breakup [2,4,9,13,16]. In the case of multiple drops interacting with each other, such as drops which are trailing one another, the flow generated by the leading drop can influence the trailing drop. This can cause changes in the drop behaviour from that of an isolated drop. Furthermore, the interaction can change drop dynamics and lead to drop collisions and coalescence which, in turn, can change the size distribution of drops in the spray. This has consequence in vaporizing and reacting fuel sprays where the size distribution of drops influence the vaporization rate which, in turn, influences the heat release rate and pollutant formation rate. This behaviour is also dependent on the properties of the liquid fuel and the ambient gas which can be expressed through non-dimensional numbers.

In this work, two numerical approaches are employed for the study. For the single drop studies, a hybrid compressible-incompressible numerical method in which the liquid phase is treated as incompressible and the gas phase as compressible is employed [13]. Finite volume discretization of the strong conservative form of the governing equations is carried out and the resulting equations are solved for both phases on an unstructured grid with interface conditions at the boundary separating the two phases. The artificial compressibility method of Chorin [1] is employed in the incompressible (liquid) phase and both the compressible flow and incompressible flow equations are solved by introducing a pseudo-time in the unsteady governing equations which allows time-marching steady state solvers to be employed. A finite volume approach with a cell-centered scheme is chosen to solve the governing equations. The convective fluxes are estimated by employing a total-variation-diminishing (TVD) scheme [15]. A second-order time accurate implicit scheme is used. The pseudo-time marching is carried out using a four-stage Runge-Kutta scheme. The geometric conservation law principle [12] is also solved numerically using the same scheme that is employed for integrating the governing equations of the two fluids. The boundaries of the computational domain consist of flow boundaries and an axisymmetry boundary. For inflow-outflow boundaries, the flow is assumed locally to be one-dimensional along the direction normal to the boundary surface element. The fluxes at the boundary surfaces are estimated using variables that are obtained by solving a local one-dimensional inviscid (LODI) system of equations [8]. Non-reflective boundary conditions are implemented in LODI by specifying amplitudes of the incoming waves to be constant in time.

The numerical method discussed above is time consuming and computational cost increases dramatically when multiple drops are considered. Hence, the multiple drop cases are simulated using the lattice-Boltzmann method (LBM) [3,10]. The key equation is the well known Boltzmann transport *equation expressed* as

$$\frac{\partial f}{\partial t} + \boldsymbol{\xi} \cdot \nabla f + \mathbf{F} \cdot \nabla_{\xi} f = \left(\frac{\partial f}{\partial t} \right)_{collision} \tag{1}$$

where *f* is the distribution function, ξ is the particle velocity, t is time, and **F** *represents* external *forces. In* single-phase flows, **F** is zero for systems without external force. In two-phase flows **F** represents the interfacial and surface tension forces. The term is modeled as

$$\mathbf{F} = -\nabla \psi + \mathbf{F_s} \cdot \tag{2}$$

where ψ is the non-ideal part of the equation of state (EOS) given by

$$\psi = p - \rho c_s^2 \tag{3}$$

We employ the Carnahan-Starling-van der Waals EOS. ψ plays an important role in phase segregation as its $p - 1/\rho$ curve

shows regions where $dp/d\rho < 0$. This represents an unstable physical situation and is the driving mechanism for keeping the phases segregated. The term $\vec{F}_s$ in Eq. (2) represents the surface tension force given by

$$\vec{F}_s = \kappa\rho\vec{\nabla}\nabla^2\rho \tag{4}$$

where κ is a surface tension parameter. It is related to the surface tension of the fluid σ by

$$\sigma = \kappa\int(\partial\rho/\partial n)^2 dn \tag{5}$$

where n is the normal to the interface. In practice, to alleviate the numerical stiffness associated with the intermolecular forces, a suitable transformation is applied to the distribution function and an index function is employed in place of density to determine different phases [3]. Note that hydrodynamic variables such as density and velocity are computed by taking moments of *f in velocity* space.

Interface Conditions for Isolated Drops

The interface conditions for the isolated drop studies will now be briefly discussed. Consider Fig. 1 which shows the interface (a) and (b) the unstructured grid developed on either side of the interface.

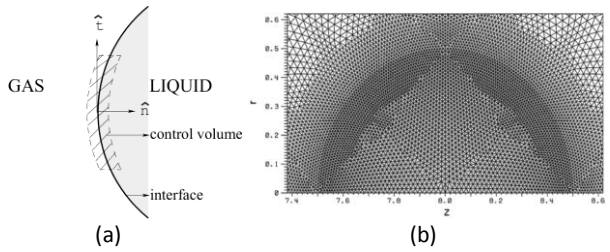

Figure 1. (a) Control volume employed to derive the interface conditions; (b) view of the grid in and around the liquid drop at the start of computation.

The assumptions made for the control volume analysis are:

i) Thickness of control volume is negligible at the interface.
ii) Mass within the interface is negligible.
iii) Velocity at the interface is subjected to the no-slip condition.

These assumptions lead to the following interface relations:

Mass:

$$\rho_l\left[(\vec{V}_l - \vec{V}_{int})\bullet\hat{n}\right] = \rho_g\left[(\vec{V}_g - \vec{V}_{int})\bullet\hat{n}\right] = \dot{m}_v \tag{4}$$

where $\dot{m}_v$ is the local vaporization mass flow rate per unit surface area and $\vec{V}_{int}$ is the interface velocity vector which is defined as the sum of the liquid phase velocity and the surface regression speed due to vaporization.

Momentum normal to the interface:

$$p_l - (\hat{n}\bullet\vec{\vec{\tau}}_l)\bullet\hat{n} = p_g - (\hat{n}\bullet\vec{\vec{\tau}}_g)\bullet\hat{n} + \sigma\kappa + \dot{m}_v(\vec{V}_g - \vec{V}_l)\bullet\hat{n} \tag{5}$$

Momentum tangential to the interface:

$$(\hat{n}\bullet\vec{\vec{\tau}}_l)\bullet\hat{t} = (\hat{n}\bullet\vec{\vec{\tau}}_g)\bullet\hat{t} + \Pi_a \tag{6}$$

where Π_a is the Marangoni stress contribution that arises due to the surface tension gradient in presence of surface temperature or composition gradients.

Energy:

$$\begin{aligned} &p_l\left(\vec{V}_l\cdot n\right) - n\cdot\left(\vec{\vec{\tau}}_l\cdot\vec{V}_l\right) + q_l\cdot n = p_g\left(\vec{V}_g\cdot n\right) \\ &-n\cdot\left(\vec{\vec{\tau}}_g\cdot\vec{V}_g\right) + q_g\cdot n + \sigma\kappa\left(\vec{V}_{\text{int}}\cdot n\right) + \dot{m}_v\left(e_g - e_l\right) \end{aligned} \tag{7}$$

where σ is the surface tension and κ is the curvature of the interface, and e is the total specific energy of gas (g) and liquid (l).

Recall that in the case of the LBM, the boundary conditions are naturally computed with á priori specification. In the section that follows, results from isolated drop studies will be presented. This will be followed in the next section with results from simulations of binary and ternary drop systems. The final section will conclude the paper.

Characterizing Non-Dimensional Parameters

The independent non-dimensional parameters that are employed for characterizing the problem are the Weber number We_g,

$$We_g = \frac{\rho_g D U^2}{\sigma}, \tag{8}$$

the Ohnesorge number Oh,

$$Oh = \frac{\mu_l}{\sqrt{\rho_l D\sigma}}, \tag{9}$$

the liquid-to-gas density ratio r,

$$r = \frac{\rho_l}{\rho_g}, \tag{10}$$

and the liquid-to-gas viscosity ratio λ,

$$\lambda = \frac{\mu_l}{\mu_g}. \tag{11}$$

In Eqs. (8) – (11), ρ is the density, μ is the dynamic viscosity, D is the drop diameter, U is its velocity, and σ is the surface tension. The subscripts l and g are for the liquid and gas, respectively. An additional parameter that may be employed is the Reynolds number Re,

$$Re = \frac{\rho UD}{\mu}. \tag{12}$$

Notice that this is not an independent parameter. We_g is a non-dimensional measure of gas inertial forces to surface tension forces. A higher We_g would suggest greater tendency to lead to deformation. Oh is a non-dimensional measure of liquid viscosity normalized by the square root of the surface tension and liquid inertial forces. A high Oh would suggest lower tendency to deform. In the case of multiple drops, these parameters can be defined for individual drops.

Isolated Drop Behavior

The parameters for the study have been selected to correspond to those of drops in high-speed atomizing sprays, such as those encountered in internal combustion engines and gas turbines. As an example, in the near-field of a diesel spray, say within 100 orifice diameters, the drop-to-gas relative velocity lies in the range of 10–100 m/ s, drop diameter is about 10–100 μm, liquid density is about 800–900 kg/m^3, and gas density varies from 15 to 40 kg/m^3. The liquid viscosity is about 2_10−3 Pa s and surface tension is about 2.2_10−2 N/m. The gas viscosity is about 1.8_10−5 Pa s. With these values, the range of the non-dimensional parameters lie in the range 20–60 for r, 80–200 for

Re_g, 1–200 for We_g, and 0.01–0.1 for Oh_l. A density ratio r of 50 is considered for the results below. The values of We_g considered are 1, 10, and 100, and Oh_l are 0.01 and 0.1. Based on the relative velocity of drop and gas, the initial Re_g is set to be 150. The transient results presented below are given in terms of non-dimensional time $t+$, where $t+$ is defined $t+=t \cdot U/(D/2)$.

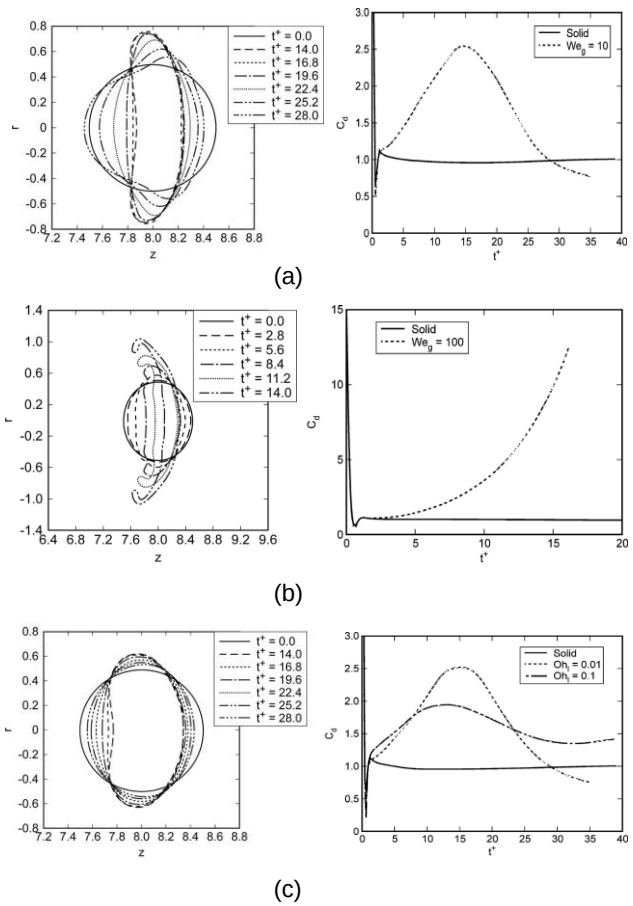

Figure 2. Computed drop shapes (left-hand column) and drag coefficients (right-hand column) as a function of non-dimensional time for (a) We_g=10, Oh = 0.01, (b) We_g=100, Oh=0.01, and (c) We_g = 10, Oh = 0.1 [14].

Computations with a We_g of 1 and Oh = 0.01 revealed that the drop behaviour was essentially that of an oscillating drop similar to that described in the classical studies of Lamb [6]. The maximum deformation of the drop was about 5.8% relative to its initial spherical shape. In prior work, it has been shown that this frequency and the decay time scale of oscillations obtained from these computations are consistent with those given by Lamb. Figure 2 (a) shows results for a case where the We_g is increased to 10. As expected, the drop deforms significantly relative to the We_g = 1 case because of the decreased influence of surface tension forces in opposing the inertial forces. The drop shape changes from oblate to prolate with oblate shapes resulting in larger drag coefficients and prolate shapes resulting in lower drag coefficients. The drag coefficient is observed to be higher by as much as a factor of 2.5 during the prolate phase. The initial decrease and then increase in drag coefficient is due to initial transients resulting from the impulsive start of the drop. The effects become dramatically pronounced when the We_g is increased to 100 (see Fig. 2(c)). In fact, in this case, it is likely that secondary breakup may occur. Drag coefficients increase by greater than a factor of 10 during the transient phase. Increasing the liquid viscosity would increase the time delay associated with liquid adjustment to external forces. As a result, the deformation effects would be expected to be less severe. Figure 2(c) shows a case where the We_g = 10, i.e. the same in Fig. 2(a), but the Oh = 0.1. Deformation is, in fact, less and the change in drag coefficient is lower.

Binary and Ternary Systems of Drops

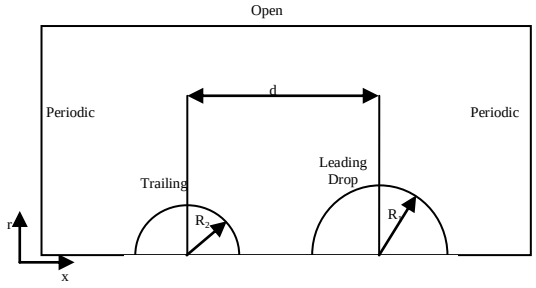

Figure 3 shows the binary drop system. The ternary drop system will add a third drop with radius R_3. The results will first be reported for a system where the drop radii are the same and density ratio r = 5, viscosity ratio λ = 5, Oh_1 = 0.025 and Oh_2 = 0.025, and $We_{g,1}$= 20 and $We_{g,2}$ = 20. The initial drop spacing d^*_{init} (d^* = d/R_1) is 3.

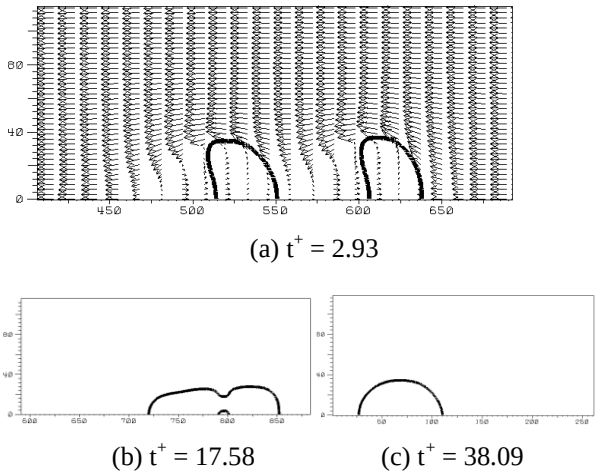

Figure 4. Binary drop interactions: $We_{g,1}$ = $We_{g,2}$ = 20, Oh_1 = Oh_2 = 0.025, R_2/R_1 = 1, d^*_{init} = 3, r = 5, and λ = 5 [5].

Differences are evident in the deformation of the drops even in the early stages (t^+=2.93) primarily because the wake of the leading drop cannot grow to its full length because of the presence of the trailing drop. With increasing time, the leading drop retains more of an oblate shape whereas the trailing drop has more of prolate shape. The oblate shape results in greater drag compared to the prolate shape as a result of which the trailing drop loses less of its momentum and runs into the leading drop leading to coalescence (t^+ = 17.58 and 38.09). Essentially, when two drops are moving in tandem, the leading drop decelerates more and deforms more. Consider next a case where the We_g of both drops are increased to 50. Figure 5 shows the results. The effects seen earlier are further accentuated. In fact, the leading drop breaks up. Compared to the isolated drop, the deformation of the leading drop is greater because of the changes in the flow field induced in the wake region. If the inter-drop spacing is increased, this effect is expected to decrease.

Next, we will consider ternary interacting drops. Two cases will be considered, one with the same conditions as the binary drop of Fig. 4 (see Fig. 6) and the other with the same condition as the

binary drop of Fig. 5. It can be seen from Fig. 6 that at t^+=5.86 the leading drop is most oblate. It then recoils to a prolate shape and the middle drop which decelerates less (see discussion of binary drop) collides and coalesces with the leading drop (see t^+=14.65). Subsequently, the third drop also coalesces (t^+=35.16) with leading drop to form a single drop (t^+=46.88). When the We_g is increased (see Fig. 7), the leading drop breaks up first, followed by the middle drop, and then the trailing drop. Detailed analysis of the results show that the leading drop decelerates fastest followed by the trailing drop and then the middle drop. The breakup of the middle drop in Fig. 7 is aided by the flow field.

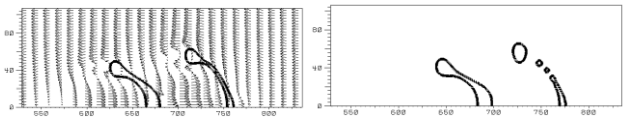

t^+ = 10.23 t^+ = 11.34

Figure 5. Binary interacting drops with We_g = 50 [5].

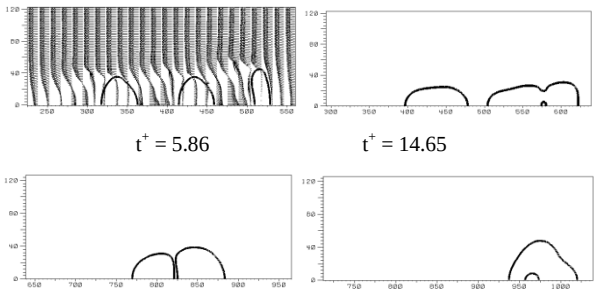

t^+ = 5.86 t^+ = 14.65

t^+ = 35.16 t^+ = 46.88

Figure 6: Ternary interacting drops; same conditions as for binary system of Fig. 4 [5].

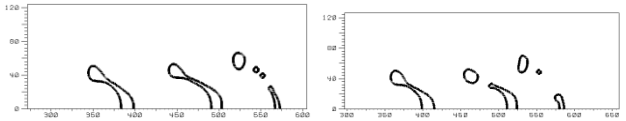

t^+ = 11.34 t^+ = 12.49

Figure 7: Ternary interacting drops; same conditions as for binary system of Fig. 5 [5].

Conclusions

Isolated drops in a decelerating flow undergo severe deformation as the We_g is increased. This deformation alters the drag coefficient of the drop dramatically. These results have consequences for the modelling of fuel sprays. Current models do not account for the changes in drag coefficient on account of deformation. Furthermore, they do not account for the changes in heat and mass transfer between the two phases on account of deformation and transient behaviour. When there is a system of drops, the drops interact with each other. For a binary interacting system, it is observed that the leading drop decelerates faster and breaks up faster (if the We_g is high enough) relative to the trailing drop. For a ternary interacting system, the leading drop decelerates faster and the middle drop decelerates slowest. As a result, the middle drop is likely to merge first with the leading drop followed by the trailing drop. The leading drops breaks up first, followed by the middle drop (because of the flow induced shear), and then the trailing drop. These changes in drop shapes in interacting systems influence the drag coefficients of individual drops and heat and mass transfer in fuel sprays. The collisions and coalescence influence the number and size distribution of drops in sprays. Properties of fuels which are factored into the relevant non-dimensional parameters influence the outcome.

References

[1] Chorin, A.J., A Numerical Method for Solving Incompressible Viscous Flow Problems, *J. Comp. Physics*, **2**, 1967, 12-26.

[2] Han, J. & Tryggvason, G., Secondary Breakup of Axisymmetric Liquid Drops II. Impulsive Acceleration, *Phys. Fluids*, **13(6)**, 2001, 1554-1565.

[3] He, X., Chen, S. & Zhang, R.A., Lattice-Boltzmann Scheme for Incompressible Multiphase Flow and its Application in Simulation of Rayleigh-Taylor Instability, *J. Comp. Phys.*, **152**, 1999, 642-663.

[4] Helenbrook, B.T. & Edwards, C.F., Quasi-Steady Deformation and Drag of Uncontaminated Liquid Drops, *Int. J. Multiphase Flow*, **28**, 2002, 1631-1657.

[5] Kumari, N. & Abraham, J., Interactions of Decelerating Drops Moving in Tandem, *Atom. Sprays*, **18**, 2008, 191-241.

[6] Lamb, H., *Hydrodynamics*, Dover, New York, 1945.

[7] Lefebvre, A.H., *Atomization and Sprays*, Hemisphere Publishing Co., CRC Press, Boca Raton, FL, 1988.

[8] Poinsot, T.J. & Lele, S.K., Boundary Conditions for Direct Simulations of Compressible Viscous Flows, *J. Comp. Phys.*, **169**, 2001, 708-759.

[9] Premnath, K.N. & Abraham, J., Simulations of Binary Drop Collisions with a Multiple-Relaxation-Time Lattice-Boltzmann Model, *Phys. Fluids*, **17(12)**, 2005, 122105.

[10] Premnath, K.N. & Abraham, J., Simulations of Binary Drop Collisions with a Multiple-Relaxation-Time Lattice-Boltzmann Model, *Phys. Fluids*, **17**, 2005, 122105.

[11] Reitz, R.D., Modeling Atomization Processes in High-Pressure Vaporizing Sprays, *Atom. Spray Tech.*,**3**, 1987, 309-337.

[12] Thomas, P.D. & Lombard, C.K., Geometric Conservation Law and its Application to Flow Computations on Moving Grids, *AIAA J.*, **17**,1979, 1030-1037.

[13] Wadhwa, A.R., Magi, V., and Abraham, J., Hybrid Compressible-Incompressible Numerical Method for Transient Drop-Gas Flows, *AIAA J.*, **43**, 2005, 1974-1983.

[14] Wadhwa, A.R., Magi, V. & Abraham, J., Transient Deformation and Drag of Decelerating Drops in Decelerating Flows, *Phys. Fluids*, **19**, 2007, 113301.

[15] Yee, H.C., A Class of High-Resolution Explicit and Implicit Shock-Capturing Methods, NASA TM 101088, Oct. 1989.

[16] Zaleski, S., Li, J. & Succi, S., Two-Dimensional Navier-Stokes Simulations of Deformation and Breakup of Liquid Patches. *Phys. Rev. Lett.*, **75(2)**, 1995, 244-247.